A Plate Motion Model of the Indo-Australian Tectonic Plate that Better Aligns with the Geodetic Coordinate System – Towards a More Precise Static Ellipsoidal Datum

J.C. McCubbine[1] A.R. Riddell[1] N. Brown[1]

1. National Geodesy Section, Space Division,
Geoscience Australia, GPO Box 378, Canberra, ACT 2601, Australia

ORCIDs:
J.C. McCubbine http://orcid.org/0000-0002-6939-1340

A.R. Riddell https://orcid.org/0000-0001-5626-8397

N. Brown https://orcid.org/0000-0001-9476-974X

Key Words: Rotation matrices, spherical polar coordinates, ellipsoidal coordinates, plate motion model, GDA2020

Plain Language Summary

We introduce a new way to study the movement of Earth's tectonic plates, using something called "ellipsoidal rotation matrices." These matrices help us understand how plates move along a path that agrees with the Earth's ellipsoidal shape. This is different to the traditional way of studying plate motion, which usually assumes the Earth is a perfect sphere.

We tested both methods by looking at the Indo-Australian tectonic plate, which is moving north-northeast at about 7 cm per year. Our findings show that the traditional, spherical method could result in slightly misrepresenting how the land is moving vertically, by up to -0.2 mm per year, since the vertical motion signal cannot be separated from the tectonic plate motion adequately. While this might not seem like much, it could matter in studies that require very accurate measurements of land height changes over time.

We verify how well each method is in capturing the real movement of the Indo-Australian tectonic plate and demonstrate that the ellipsoidal method is more accurate.

Abstract

We present a class of "ellipsoidal rotation matrices" which can be used to characterise tectonic plate motion; where geocentric Cartesian coordinates travel along paths tangential to the ellipsoid. We contrast them with conventional Euler pole plate motion models which are more closely aligned with spherical coordinate systems and inherently induce a change in geodetic ellipsoidal height. We demonstrate the use of each in the Indo-Australian tectonic plate setting, which is known to move approximately 7 cm/yr in a north-northeast direction. Geocentric Datum of Australia 2020 (GDA2020) coordinates are "plate-fixed" static coordinates obtained using a conventional Euler pole plate motion model to align time dependent coordinates with the 2014 realisation of the International Terrestrial Reference Frame (ITRF) at the epoch 2020.0. We show that this Euler pole plate motion model can introduce ellipsoidal height velocities of up to -0.2 mm/yr. This is small but systematic, so pertinent for consideration with high accuracy vertical land motion studies using GDA2020 coordinates. We further investigate the comparative statistical accuracy of conventional Euler pole and the ellipsoidal models with respect to characterising plate motion captured in high quality GNSS data.

1. Introduction

Spherical Earth approximations are ubiquitous in geodetic calculations. For example, regional evaluations of Stokes integral to determine the geoid from gravity anomalies (e.g. Heiskanen & Moritz, 1967, Claessens, 2006 and Featherstone et al., 2018); using the degree-1 spherical harmonic coefficients to represent geocentre motion (e.g. Swenson et al., 2008; Cheng et al., 2010; and Sun et at., 2016); and in estimating co- and post-seismic crustal deformation (e.g. Pollitz, 1997; and Nield et al., 2022). Here we discuss the impact of the spherical Earth approximation on vertical land motion studies, when using Euler pole models to parameterise the motion of tectonic plates (e.g. Cox and Hart, 1986 and ICSM, 2021) to establish a static ellipsoidal coordinate datum.

An Euler pole model is a coordinate transformation that utilises conventional rotation matrices to propagate coordinates over paths tangent to a local sphere (Fig 1 (a)). They are perfectly suited to modelling rigid body motion, which is a commonly held assumption for the motion of tectonic plates (e.g. Cox and Hart, 1986, Cuffarao et al 2008). During the transformation, the radius, r, from the geocentre is fixed and the Euclidean distance between any two points is perfectly preserved.

Euler pole models can be used to parameterise tectonic plate motion e.g. to align time dependent coordinates with a static geodetic datum as with the Australian Plate Motion Model and Geocentric Datum of Australia 2020.They only act on the Spherical Polar coordinates θ and λ (Table 1). For this reason, simply due to the difference in the geographic coordinate systems (Table 1), any north/south motion captured by the model induces a change in the geodetic height, Δh (c.f. Fig 1 (b)), albeit usually at the millimetre level.

Table 1. Commonly used geographic coordinate systems

Cartesian	Spherical polar	Geodetic	Ellipsoidal

x	$r\cos\theta\cos\lambda$	$(v+h)\cos\phi\cos\lambda$	$\sqrt{\mu^2+E^2}\cos\beta\cos\lambda$
y	$r\cos\theta\sin\lambda$	$(v+h)\cos\phi\sin\lambda$	$\sqrt{\mu^2+E^2}\cos\beta\,sin\lambda$
z	$r\sin\theta$	$(v(1-e^2)+h)\sin\phi$	$\mu\sin\beta$

In Table 1, r is the radius of the point from the Earth's centre, θ, ϕ and β are the Spherical, Geodetic and Ellipsoidal latitudes (Fig 1) and λ is the longitude. For the Geodetic and Ellipsoidal coordinates, a "reference ellipsoid" is used with polar radius a and equatorial radius b, e^2 is the first numerical eccentricity (Eq. 1 a), E^2 (Eq. 1 b) is the linear eccentricity and v is the prime vertical radius of curvature (Eq. 1 c) (Claessens, 2006).

$$e^2 = \frac{a^2 - b^2}{a^2} \tag{1 a}$$

$$E^2 = a^2 - b^2 \tag{1 b}$$

$$v = \frac{a}{\sqrt{1-e^2\sin^2(\phi)}} \tag{1 c}$$

$$\boldsymbol{x_{ENU}} = \begin{bmatrix} -\sin\lambda & \cos\lambda & 0 \\ -\cos\lambda\sin\phi & -\sin\lambda\sin\phi & \cos\phi \\ \cos\lambda\cos\phi & \sin\lambda\cos\phi & \sin\phi \end{bmatrix} \boldsymbol{x} \tag{1 d}$$

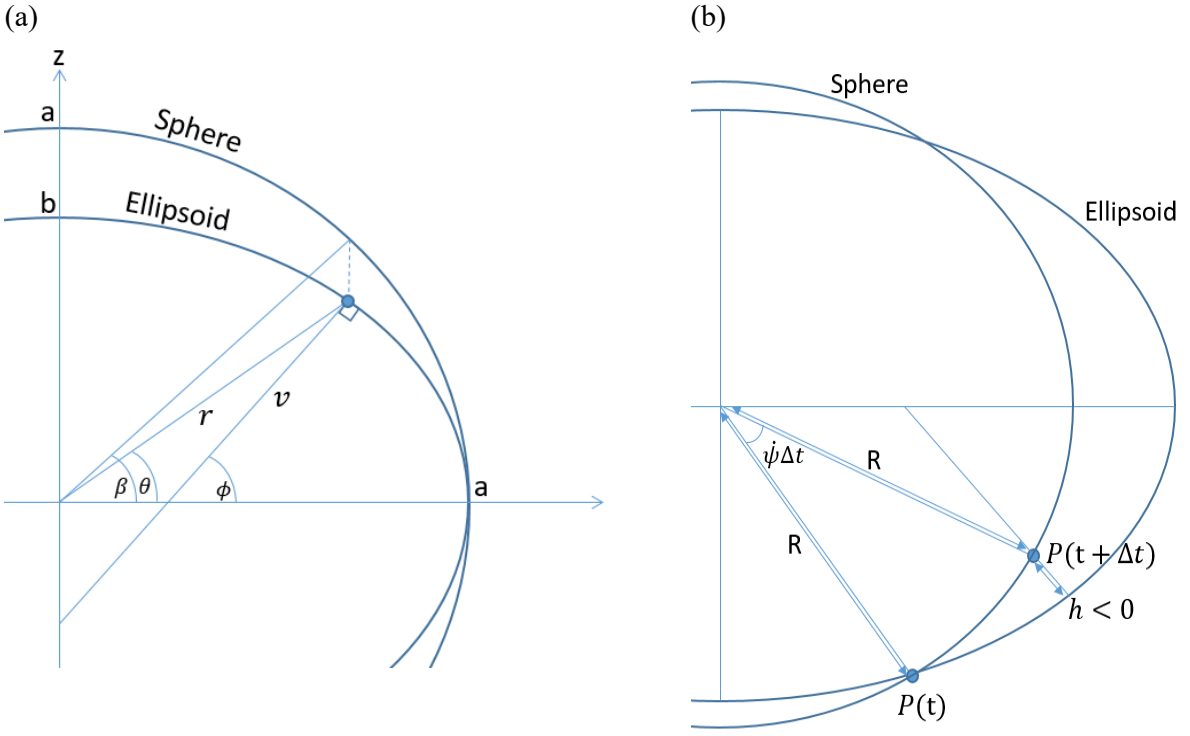

Figure 1 (a) Depiction of 3 kinds of geographic latitude, θ, ϕ and β i.e. the spherical, geodetic and Ellipsoidal latitude respectively. (b) Graphical depiction of geodetic height changes induced by rotation matrices aligned with the spherical coordinate system. A point on the ellipsoid, P(t) has been rotated northwards by and angle $\dot{\Psi}\Delta t$.

The Australian tectonic plate moves north-northeast at approximately 7 cm per year (Fig 2). The Australian Plate Motion Model (APMM) (ICSM, 2021 & 2020) is a spherical Earth Centred Earth Fixed (ECEF) model that is aligned to ITRF2014. It can be used to propagate coordinates situated on the Australian continent back and forth through time to facilitate the alignment of spatial datasets that have been obtained at different epochs. The current published APMM underpins the transformation used to produce static Geocentric Datum of Australia (GDA2020) and time dependent Australian Terrestrial Reference Frame (ATRF) coordinates (ICSM, 2021). It is a conventional Euler pole tectonic plate motion model and has a validity period of 30 years, from epoch 2005.0 to 2035.0 (ICSM, 2021). In Sec. 3 we present the changes in geodetic heights (up to 5 mm) induced by the model over this time period. This change in height is small, only 0.2 mm/yr, and uncertainties of this size have been deemed insignificant in other studies investigating the usage of broad scale tectonic plate motion models (e.g. Altimimi et al, 2017). However, in the context of the Global Geodetic Observing System which has set aspirational goals for an accurate and stable reference frame at the levels of 1 mm and 0.1 mm/yr – we consider this to be pertinent for further consideration.

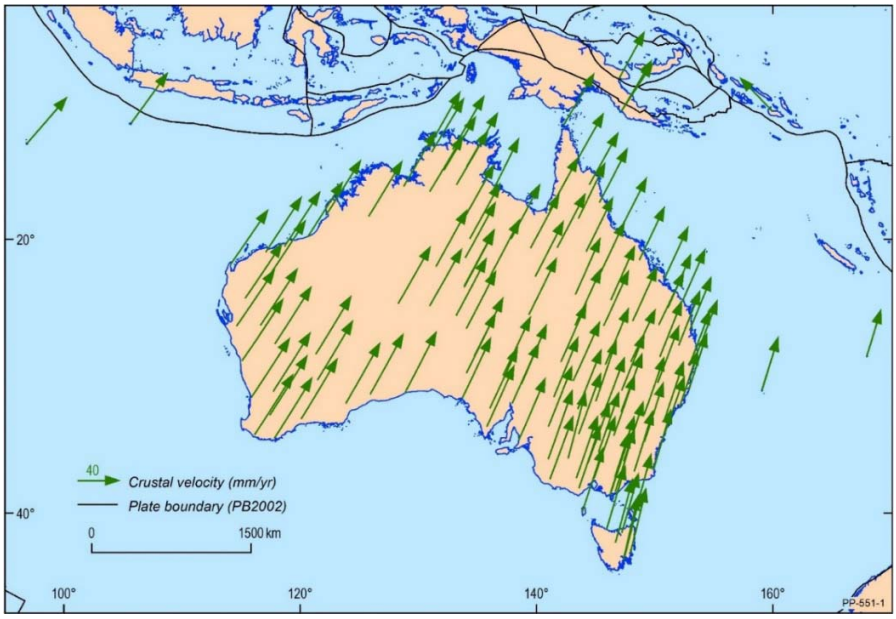

Figure 2: The Australian tectonic plate motion, as observed at GNSS sites, moving approximately 7 cm/yr north-northeast direction. (ICSM, 2021)

Blewitt (2015) states that "…true plate motions (for the part of plates exposed on the Earth's surface) are on average gravitationally horizontal (with respect to the geoid), then on average, the motion must also be horizontal with respect to the reference ellipsoid…". This sits in contrast with the convention of using Euler pole plate motion models to generalise continental scale land motion. Towards this, we have formulated a new class of so called "ellipsoidal rotation matrices" which propagate points over paths tangent to the ellipsoid. All results presented in sections 3 and 4 use the GRS80 ellipsoid values for the parameters describes in equations 1 a), b) and c). These ellipsoidal rotation matrices act only on the Ellipsoidal coordinates β and λ of a point (i.e. $\mu = const.$ under the transformation). The Ellipsoidal

coordinates are closely aligned with the Geodetic coordinates ϕ and λ, so when used to generalise tectonic plate motion, the ellipsoidal rotation matrices alleviate the aforementioned change in Geodetic height, h, induced by their Euler pole model counterparts. However, we acknowledge that this comes at the expense of violating the assumption that the tectonic plates are rigid bodies. Under ellipsoidal rotations, points below the equator will separate in an east west direction as they move northward.

We explore the use of both spherical and ellipsoidal rotation matrices to parameterise the Indo-Australian tectonic plate motion captured in the Cartesian velocities, provided in high quality GNSS data and report on the residuals of the fitted plate motion models in the context of the accuracy of the underlying data informing it. Vertical velocities appear to be better preserved under the ellipsoidal rotations and violating the assumption of rigid body motion does not appear to result in a statistically significant difference in the accuracy of the fitted plate motion models.

2. Rotation matrices

Rotation matrices can be used to evolve a linear dynamical system backward and forward through time (Eq. 2 a). Here, we consider "spherical rotation matrices" to be those which evolve points, $\boldsymbol{x}_t$ over paths that are tangent to a local sphere, centred at the origin with radius $\left|\left|\boldsymbol{x}_t\right|\right|_2$, and ellipsoidal rotation matrices to be those which evolve points over paths tangent to a local ellipsoid.

$$\boldsymbol{x}_{t+\Delta t} = (I + K\Delta t)\boldsymbol{x}_t \qquad (2\text{ a})$$

In Eq. (2 a), $\boldsymbol{x}_t$ and $\boldsymbol{x}_{t+\Delta t}$ are 3×1 vectors of Cartesian coordinates at times t and $t + \Delta t$ respectively where Δt is a small increment of time and I is a 3×3 identity matrix.

2.1 Spherical rotation matrices

In the case of spherical rotation matrices, K (Eq. 2 a), a 3×3 skew symmetric matrix which is characterised by an Euler pole, $\boldsymbol{u}$ and constant rotation rate $\dot{\psi}$. The Euler pole, $\boldsymbol{u}$ is a unit vector that passes through the origin which acts as the axis about which points rotate. It is parameterized by a spherical polar latitude θ and longitude λ (Eq. 2.1 a).

Assuming a small rotation $\dot{\psi}$ and time increment, Δt, Eq. (2.1 c) is the small angle approximation to the full Rodrigues rotation formula (Eq. 2.1 b). The small angle approximation is the "3 – parameter" spherical rotation matrix, with parameters $[\dot{\psi}\, u_1\, , \dot{\psi}\, u_2\, , \dot{\psi}\, u_3]$.

$$\boldsymbol{u} = \begin{bmatrix} cos(\theta)cos(\lambda) \\ cos(\theta)sin(\lambda) \\ sin(\theta) \end{bmatrix} \qquad (2.1\text{ a})$$

$$R_\theta(\dot{\psi}\Delta t) = I + \begin{bmatrix} 0 & -u_3 & u_2 \\ u_3 & 0 & -u_1 \\ -u_2 & u_1 & 0 \end{bmatrix} \sin(\dot{\psi}\Delta t) + \begin{bmatrix} 0 & -u_3 & u_2 \\ u_3 & 0 & -u_1 \\ -u_2 & u_1 & 0 \end{bmatrix}^2 (1 - \cos(\dot{\psi}\Delta t)) \quad (2.1\text{ b})$$

$$R_\theta(\dot{\psi}\Delta t) \approx I + \begin{bmatrix} 0 & -u_3 & u_2 \\ u_3 & 0 & -u_1 \\ -u_2 & u_1 & 0 \end{bmatrix} \dot{\psi}\Delta t \quad (2.1\text{ c})$$

2.2 Rotation matrices consistent with the geographic ellipsoidal coordinate system

Özdemir (2016) provides, so-called, ellipsoidal rotation matrices. The form of the matrices is similar to that of the spherical rotation matrix. For an oblate ellipsoid with semi-major axis a and semi-minor axis b, the rotation matrix is parametrised by an axis $\boldsymbol{v}$ (Eq. 2.2 a), and an angle ψ, and is given by Eq. (2.2 b) (following Özdemir, 2016).

$$\boldsymbol{v} = \begin{bmatrix} a\,cos(\beta)cos(\lambda) \\ a\,cos(\beta)sin(\lambda) \\ b\,sin(\beta) \end{bmatrix} \quad (2.2\text{ a})$$

$$R_\beta(\psi) = \begin{bmatrix} \frac{v_1^2}{a^2} + \left(1 - \frac{v_1^2}{a^2}\right)\cos(\psi) & -Dv_3a^2\sin(\psi) - \frac{v_1v_2}{a^2}(\cos(\psi) - 1) & Dv_2a^2\sin(\psi) - \frac{v_1v_3}{b^2}(\cos(\psi) - 1) \\ Dv_3a^2\sin(\psi) - \frac{v_1v_2}{a^2}(\cos(\psi) - 1) & \frac{v_2^2}{a^2} + \left(1 - \frac{v_2^2}{a^2}\right)\cos(\psi) & -Dv_1a^2\sin(\psi) - \frac{v_2v_3}{b^2}(\cos(\psi) - 1) \\ -Dv_2b^2\sin(\psi) - \frac{v_1v_3}{a^2}(\cos(\psi) - 1) & Dv_1b^2\sin(\psi) - \frac{v_2v_3}{b^2}(\cos(\psi) - 1) & \frac{v_3^2}{b^2} + \left(1 - \frac{v_3^2}{b^2}\right)\cos(\psi) \end{bmatrix} \quad (2.2\text{ b})$$

$D = \frac{1}{\sqrt{a^4b^2}}$ is the scalar product constant (Özdemir, 2016). Under the small angle approximation with the rotation angle $\psi = \dot{\psi}\Delta t$, Eq. (2.2 c) is an ellipsoidal 3-parameter rotation matrix with parameters $[\dot{\psi}\,v_1\,, \dot{\psi}\,v_2\,, \dot{\psi}\,v_3]$.

$$R_\beta(\dot{\psi}\Delta t) \approx I + \begin{bmatrix} 0 & -Da^2v_3\dot{\psi} & Da^2v_2\dot{\psi} \\ Da^2v_3\dot{\psi} & 0 & -Da^2v_1\dot{\psi} \\ -Db^2v_2\dot{\psi} & Db^2v_1\dot{\psi} & 0 \end{bmatrix} \Delta t \quad (2.2\text{ c})$$

For points located on the surface of the ellipsoid, these rotation matrices propagate points $\boldsymbol{x_t}$ over paths tangent to the ellipsoid, i.e. with Ellipsoidal coordinates $(\beta_t, \lambda_t, \mu = b)$. However, points located above or below the ellipsoid (i.e. $\mu \neq b$), will follow paths consistent with the coordinates described by Eq. (2.2.d). k is a scaling factor which rescales the ellipsoid (defined by parameters a and b) in the spherical radial direction, to an ellipsoid with the same eccentricity. These paths do not coincide with any well-recognised geographic coordinate system (e.g. those in Table 1). For this reason the usage of Eq. 2.2 c will result in a change in the geodetic height of the point (albeit much smaller than that of an Euler pole model).

$$\boldsymbol{x_t} = \begin{bmatrix} x_t \\ y_t \\ z_t \end{bmatrix} = \begin{bmatrix} ka\cos(\beta_t)\cos(\lambda_t) \\ ka\cos(\beta_t)\sin(\lambda_t) \\ kb\sin(\beta_t) \end{bmatrix} \tag{2.2 d}$$

To rectify this, Eq. (2.2 e-h) extends the formulae provided by Özdemir (2016), giving a class of rotation matrices which can propagate coordinates over paths consistent with more conventional Ellipsoidal coordinates ($\beta_t, \lambda_t, \mu = const.$) (e.g. Eq. (2.3 e)). This is accomplished by further parameterising the rotation matrix and "Euler pole" with the Ellipsoidal coordinate, μ of the point being rotated (i.e. $\boldsymbol{x_t} = (\beta_t, \lambda_t, \mu)$).

The full rotation matrix and small angle approximation are given by Eq. (2.3 f) and Eq. (2.3 g), where $D = \frac{1}{\sqrt{(\mu^2+E^2)^2\,\mu^2}}$. Similarly to Eq. (2.2 g) this rotation matrix is a 3 parameter model – with parameters $[\dot{\psi}\,v_1\,, \dot{\psi}\,v_2\,, \dot{\psi}\,v_3]$.

$$\boldsymbol{v} = \begin{bmatrix} \sqrt{\mu^2+E^2}\,cos(\hat{\beta})cos(\hat{\lambda}) \\ \sqrt{\mu^2+E^2}\,cos(\hat{\beta})sin(\hat{\lambda}) \\ \mu\,sin(\hat{\beta}) \end{bmatrix} \tag{2.3 e}$$

$$R_\beta(\mu,\psi) = \begin{bmatrix} \frac{v_1^2}{\mu^2+E^2} + \left(1 - \frac{v_1^2}{\mu^2+E^2}\right)\cos(\psi) & -Dv_3(\mu^2+E^2)\sin(\psi) - \frac{v_1v_2}{\mu^2+E^2}(\cos(\psi)-1) & Dv_2(\mu^2+E^2)\sin(\psi) - \frac{v_1v_3}{\mu^2}(\cos(\psi)-1) \\ Dv_3(\mu^2+E^2)\sin(\psi) - \frac{v_1v_2}{\mu^2+E^2}(\cos(\psi)-1) & \frac{v_2^2}{\mu^2+E^2} + \left(1 - \frac{v_2^2}{\mu^2+E^2}\right)\cos(\psi) & -Dv_1(\mu^2+E^2)\sin(\psi) - \frac{v_2v_3}{\mu^2}(\cos(\psi)-1) \\ -Dv_2\mu^2\sin(\psi) - \frac{v_1v_3}{\mu^2+E^2}(\cos(\psi)-1) & Dv_1\mu^2\sin(\psi) - \frac{v_2v_3}{\mu^2}(\cos(\psi)-1) & \frac{v_3^2}{\mu^2} + \left(1 - \frac{v_3^2}{\mu^2}\right)\cos(\psi) \end{bmatrix} \tag{2.3 f}$$

$$R_\beta(\mu,\psi) \approx I + \begin{bmatrix} 0 & -D(\mu^2+E^2)v_3 & D(\mu^2+E^2)v_2 \\ D(\mu^2+E^2)v_3 & 0 & -D(\mu^2+E^2)v_1 \\ -D\mu^2v_2 & D\mu^2v_1 & 0 \end{bmatrix} \dot{\psi}\Delta t \tag{2.3 g}$$

Or similarly by writing,

$$\hat{\boldsymbol{v}} = \begin{bmatrix} cos(\hat{\beta})cos(\hat{\lambda}) \\ cos(\hat{\beta})sin(\hat{\lambda}) \\ sin(\hat{\beta}) \end{bmatrix} \tag{2.3 h}$$

and,

$$\hat{R}_\beta(\mu,\psi) \approx$$

$$I + \begin{bmatrix} 0 & -D(\mu^2+E^2)\mu\,\hat{v}_3 & D(\mu^2+E^2)\sqrt{\mu^2+E^2}\,\hat{v}_2 \\ D(\mu^2+E^2)\mu\hat{v}_3 & 0 & -D(\mu^2+E^2)\sqrt{\mu^2+E^2}\,\hat{v}_1 \\ -D\mu^2\sqrt{\mu^2+E^2}\,\hat{v}_2 & D\mu^2\sqrt{\mu^2+E^2}\,\hat{v}_1 & 0 \end{bmatrix} \dot{\psi}\Delta t$$

(2.3 i)

gives a 3 parameter model with parameters $\hat{v}_1, \hat{v}_2, \hat{v}_3$. Note that as E tends towards zero 2.3 i. tends towards the conventional Euler pole model. i.e. the ellipsoidal rotation matrix reduce to the spherical model when the ellipsoid has a zero eccentricity.

3. The Australian Plate Motion Model used to produce GDA2020 coordinates

The Australian Plate Motion Model (APMM) is a "3-parameter Euler pole plate motion model" and corresponds to a "spherical rotation matrix". The parameters of the APMM are provided in the GDA2020 technical manual (ICSM, 2021) and here in Table 2. They were fitted to Global Navigation Satellite System (GNSS) time series data at 109 Australian Fiducial Network (ICSM, 2021) sites by least squares. The characteristic parameters of the APMM are provided as the rotation rate in arc seconds multiplied by the Euler pole constituents (i.e. the three parameters $[\dot{\psi}\,u_1\,, \dot{\psi}\,u_2\,, \dot{\psi}\,u_3]$).

Table 2: Parameters of the APMM provided in the GDA2020 Technical Manual (ICSM, 2021).

Parameter	$u_1\dot{\psi}\frac{648000}{\pi}$	$u_2\dot{\psi}\frac{648000}{\pi}$	$u_3\dot{\psi}\frac{648000}{\pi}$
Parameter value	0.00150379	0.00118346	0.00120716

The APMM rotation matrix is given by Eq. (3.1). The scale factor $\frac{\pi}{648000}$ converts the rotation rates from arc seconds per year to radians per year.

$$R_\theta(\Delta t) \approx I + \frac{\pi}{648000}\begin{bmatrix} 0 & -0.00120716 & 0.00118346 \\ 0.00120716 & 0 & -0.00150379 \\ -0.00118346 & 0.00150379 & 0 \end{bmatrix} \Delta t$$

(3.1)

To numerically investigate the change in geodetic height induced by the APMM over the Australian mainland, we consider a grid of points on the surface of the ellipsoid covering the region 10° to 60° S and 90° to 170° E. Treating these points as time dependent coordinates at epoch 2005.0, the coordinates have been propagated forward in time using the APMM, to epoch 2035.0 (i.e. $\Delta t = 30$). These epochs were chosen since 2005.0 to 2035.0 is specified to be the period that the APMM is considered to be valid (ICSM, 2021).

Fig (3 a) shows the difference between the geodetic heights at epochs 2005.0 and 2035.0. The height differences range from 2 to 6 mm. Linear vertical velocities

have been crudely estimated to be between -0.06 and $-0.2\,\frac{mm}{yr}$ (Fig. 3 b), by dividing the height displacement (of Fig 3 b) by 30 years. This vertical velocity rate is small but a signal of this amplitude is detectable in measurements made with modern positioning equipment over long enough time periods. e.g. many velocity estimates in the ITRF2014 solution (Altamimi et. al, 2016) have accuracies below 0.05 mm/yr. If this effect is disregarded in local scale studies of vertical land motion, it could be falsely interpreted as subsidence.

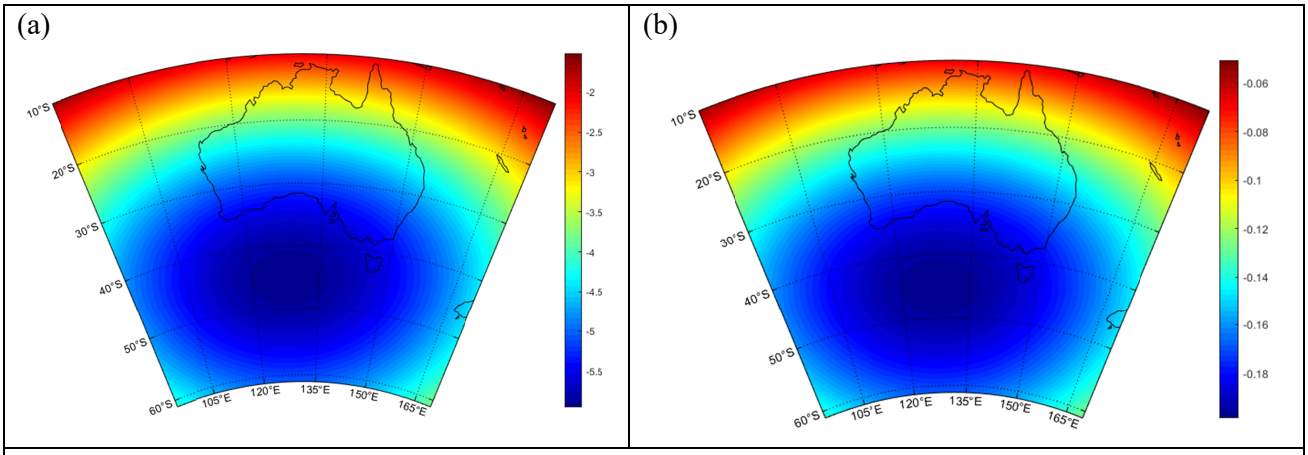

Figure 1 (a) Difference (in mm) between the height of time dependent GRS80 ellipsoidal coordinates at 2035.0 and 2005.0 (former minus the latter) derived from GDA2020 coordinates using the APMM.(b) Rate of change in height (in mm/yr) introduced by the APMM.

4. Rotation matrices fitted to the data points in the ITRF2014 solution over the Indo-Australian Tectonic Plate

Eight hundred and forty one (841) GNSS data points on the Indo-Australian tectonic plate composed of all data from the ITRF2014 solution (Altamimi et al., 2016) supplement with the Geoscience Australia data holdings (Geoscience Australia, 2021) into a single dataset. Each data point consists of an Earth centre Earth fixed X, Y, Z position and respective linear velocity estimates, $\dot{X}, \dot{Y}, \dot{Z}$ in m/yr. Of the 841 data points, a subset of 65 of them have positions with standard deviation of less than 0.5 mm and velocities with standard deviations of less than 0.05 mm/yr. We consider this subset of 65 data points to be of "high-quality" (Fig. 4), noting that the Global Geodetic Observing System has set aspirational goals for an accurate and stable reference frame at the levels of 1 mm and 0.1 mm/yr, respectively (Gross et al., 2009). The statistics of the velocity estimates in the GNSS data are given in Table 4. In particular, it shows that, before any generalised plate motion is accounted for, both the 65 "high-quality" data points have mean, eastward velocities of ~24 mm/yr and northward velocities of ~56 mm/yr (and similarly for the total 841 sites). This is in agreement with the approximate 7 cm/yr north/northeast velocity of the generalised plate motion model noted in ICSM (2021).

Table 4 - Statistics of the GNSS velocity data on the Indo-Australian tectonic plate in a local ellipsoidal East/North/Up frame of reference.

Statistic	East	North	Up
All 841 sites			
Mean (mm/yr)	22.580	55.094	-2.015
Min (mm/yr)	-128.714	-91.925	-278.068
Max (mm/yr)	72.305	149.906	117.556
STD (mm/yr)	10.488	9.126	14.999
The 65 high-quality sites			
Mean (mm/yr)	24.964	56.081	-0.811
Min (mm/yr)	-1.990	38.226	-1.993
Max (mm/yr)	39.047	59.432	0.7865
STD (mm/yr)	10.388	4.265	0.446

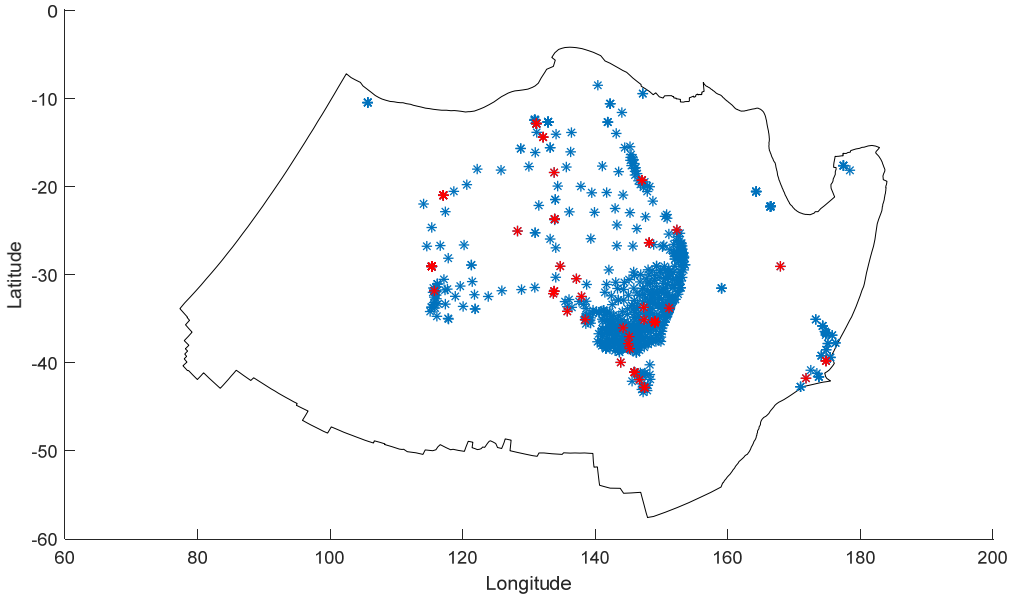

Figure 4 – All (841) sites in the GNSS data within the boundary of the Indo-Australian tectonic plate, shown as blue stars – (65) sites with positions with STD < 0.5 mm and Velocity STD < 0.05 mm/yr as red stars – black boundary line identifies the edge of the Indo-Australian tectonic plate (from Bird 2003).

Plate motion models, of the spherical and ellipsoidal kinds, can be fitted to the linear velocity estimates by least squares (e.g. for the spherical type; Cuffaro, M., Caputo, M., and Doglioni, C., 2008; Altamimi et al., 2017). Table (5) shows the parameters and statistics of the residuals (in a local ENU coordinate system) of a spherical rotation matrix fitted to (i) the full set of positions and velocity values extracted from the ITRF2014 solution (Altamimi et al., 2017) within the boundary of the Indo-Australian tectonic plate provide by Bird (2003) (Fig 4) and (ii) of a spherical rotation matrix fitted to the 65 sites with high-quality position and velocity data. Similarly, Table (6) shows the parameters and statistics of the residuals (in a local ENU coordinate system) for the fitted ellipsoidal rotation matrices (for the formulation present here in Eq. 2.3 i and for the more simplistic model of Eq. 2.3 c).

Table 5 - parameters and statistics of the residuals for a spherical rotation matrix fitted to GNSS position and velocity data velocity.

Parameter	$u_1\dot{\psi}\frac{648000}{\pi}$	$u_2\dot{\psi}\frac{648000}{\pi}$	$u_3\dot{\psi}\frac{648000}{\pi}$
Using all 841 sites			
Parameter value	0.00152614	0.00117149	0.00121342
Residuals	***East***	***North***	***Up***
Mean (mm/yr)	0.101	-0.213	-1.855
Min (mm/yr)	-149.074	-150.246	-277.887
Max (mm/yr)	37.136	92.624	177.744
STD (mm/yr)	6.439	8.101	14.999
Using the 65 high-quality sites			
Parameter value	0.00152575	0.00117342	0.00121387
Residuals	***East***	***North***	***Up***
Mean (mm/yr)	0.102	-0.185	-0.651
Min (mm/yr)	-2.541	-2.116	-1.819
Max (mm/yr)	0.863	0.322	0.905
STD (mm/yr)	0.627	0.407	0.435

Table 6 - parameters and statistics of the residuals for ellipsoidal rotation matrices of the form of Eq. 2.3 I and c fitted to GNSS position and velocity data.

Parameter	$\hat{v}_1\dot{\psi}\frac{648000}{\pi}$	$\hat{v}_2\dot{\psi}\frac{648000}{\pi}$	$\hat{v}_3\dot{\psi}\frac{648000}{\pi}$
Geodetic Coordinate Ellipsoidal Rotation Matrix Eq. 2.3 i			
Using all 841 sites			
Parameter value	0.00152812	0.00117384	0.00121571
Residuals	**East**	**North**	**Up**
Mean (mm/yr)	0.077	-0.223	-2.015
Min (mm/yr)	-149.095	-150.266	-278.068
Max (mm/yr)	37.073	92.581	117.556
STD (mm/yr)	6.439	8.099	14.999
Using the 65 high-quality sites			
Parameter value	0.00152799	0.00117569	0.00121584
Residuals	**East**	**North**	**Up**
Mean (mm/yr)	0.0791	-0.194	-0.811
Min (mm/yr)	-2.455	-2.167	-1.994
Max (mm/yr)	0.861	0.298	0.787
STD (mm/yr)	0.613	0.421	0.446
Geodetic Coordinate Ellipsoidal Rotation Matrix Eq. 2.3 c			
Using all 841 sites			
Parameter value	0.00152970	0.00117464	0.00121050
Residuals	**East**	**North**	**Up**
Mean (mm/yr)	0.089	-0.218	-1.935
Min (mm/yr)	-149.088	-150.256	-277.978
Max (mm/yr)	37.105	92.602	117.650
STD (mm/yr)	6.439	8.010	14.999
Using the 65 high-quality sites			
Parameter value	0.0015294	0.0011765	0.0012107
Residuals	**East**	**North**	**Up**
Mean (mm/yr)	0.091	-0.190	-0.731
Min (mm/yr)	-2.498	-2.141	-1.906

Max (mm/yr)	0.862	0.303	0.846
STD (mm/yr)	0.620	0.413	0.440

To investigate the effect of mitigating any influence the geodetic height velocities may have on the fitted spherical and ellipsoidal plate motion models, we first rotated the GNSS derived Cartesian velocities of each data point into a local ENU reference frame, set the "Up" velocity to zero, then transformed the velocities back into Cartesian velocities. Spherical and ellipsoidal rotation matrices were then fitted to these "2D only" velocity data. Tables (7) and (8) show the parameters and residuals of spherical and ellipsoidal rotation matrices fitted to these velocity data.

Table 7 - parameters and statistics of the residuals for a spherical rotation matrix fitted to GNSS positions with geodetic height velocities set to zero before fitting.

Parameter	$u_1\dot{\psi}\frac{648000}{\pi}$	$u_2\dot{\psi}\frac{648000}{\pi}$	$u_3\dot{\psi}\frac{648000}{\pi}$
Using all 841 ITRF2014 sites			
Parameter value	0.00152732	0.00116768	0.00121270
Residuals	***East***	***North***	***Up***
Mean (mm/yr)	0.169	-0.139	0.160
Min (mm/yr)	-148.996	-150.182	0.057
Max (mm/yr)	37.174	92.696	0.188
STD (mm/yr)	6.439	8.102	0.030
Using the 65 high-quality ITRF2014 sites			
Parameter value	0.00152817	0.00116893	0.00121331
Residuals	***East***	***North***	***Up***
Mean (mm/yr)	0.188	-0.130	0.159
Min (mm/yr)	-2.473	-1.984	0.0862
Max (mm/yr)	0.967	0.393	0.188
STD (mm/yr)	0.633	0.401	0.028

Table 8 - parameters and statistics of the residuals for the ellipsoidal rotation matrices of the form of Eq. 2.3 I and c fitted to GNSS positions with geodetic height velocities set to zero before fitting.

Parameter	$\hat{v}_1\dot{\psi}\frac{648000}{\pi}$	$\hat{v}_2\dot{\psi}\frac{648000}{\pi}$	$\hat{v}_3\dot{\psi}\frac{648000}{\pi}$
Geodetic Coordinate Ellipsoidal Rotation Matrix Eq. 2.3 i			
Using all 841 sites			
Parameter value	0.00152932	0.00117009	0.00121499
Residuals	**East**	**North**	**Up**
Mean (mm/yr)	0.1445	-0.1516	0.000
Min (mm/yr)	-149.0172	-150.2038	0.000
Max (mm/yr)	37.110	92.651	0.000
STD (mm/yr)	6.439	8.099	0.000
Using the 65 high-quality sites			
Parameter value	0.00153040	0.00117129	0.00121526
Residuals	**East**	**North**	**Up**
Mean (mm/yr)	0.165	-0.140	0.000
Min (mm/yr)	-2.386	-2.038	0.000
Max (mm/yr)	0.965	0.356	0.000
STD (mm/yr)	0.619	0.413	0.000
Geodetic Coordinate Ellipsoidal Rotation Matrix Eq. 2.3 c			
Using all 841 sites			

Parameter value	0.00153089	0.00117085	0.00120978
Residuals	**East**	**North**	**Up**
Mean (mm/yr)	0.157	-0.146	0.080
Min (mm/yr)	-149.007	-150.193	0.028
Max (mm/yr)	37.142	92.673	0.094
STD (mm/yr)	6.439	8.101	0.015
Using the 65 high-quality sites			
Parameter value	0.00153186	0.00117208	0.00121021
Residuals	**East**	**North**	**Up**
Mean (mm/yr)	0.176	-0.135	0.080
Min (mm/yr)	-2.429	-2.012	0.043
Max (mm/yr)	0.966	0.367	0.094
STD (mm/yr)	0.625	0.406	0.014

4.1 Discussion

In Table 4, there is a mean geodetic vertical velocity ("Up") of -0.811 mm/year which is consistent with the results presented by Riddell et al. (2020) and Rezvani et al (2022), where the mean rate of subsidence is reasonably spatially coherent and cannot be explained by Glacial Isostatic Adjustment alone. These mean velocities have variations across the high-quality data points of $\pm$ 10.388 mm/yr in the East direction, $\pm$ 4.265 mm/yr in the North direction and $\pm$ 0.446 mm/yr in the Up direction.

The residuals of the high-quality data, after the fitted "conventional Euler pole plate motion model" (i.e. the spherical rotation matrix) is removed, have a mean of 0.10 mm/yr and a standard deviation of 0.63 mm./yr, in the East direction and a mean of -0.19 mm/yr and a standard deviation of 0.41 mm./yr in the North direction. Similarly for the ellipsoidal model (of the "Geodetic Coordinate Ellipsoidal Rotation Matrix Eq. 2.3 i" type), the residuals have a mean of 0.07 mm/yr and a standard deviation of 0.61 mm/yr, in the East direction and a mean of -0.19 mm/yr and a standard deviation of 0.42 mm./yr in the North direction. For both cases, the mean of the East and North residuals are not significantly different from 0 at the 95% confidence level (crudely using a "t-test" with T-statistics of $\left\{\frac{0.1}{\frac{0.63}{\sqrt{64}}} = 0.02, \frac{0.19}{\frac{0.41}{\sqrt{64}}} = 0.06, \frac{0.07}{\frac{0.61}{\sqrt{64}}} = 0.01, \frac{0.19}{\frac{0.42}{\sqrt{64}}} = 0.06,\right\}$) given their respective residual standard deviation. An f-test (with T-statistics of $\left\{\frac{0.63^2}{0.61^2} = 1.07, \frac{0.63^2}{0.61^2} = 1.05\right\}$) with 64 degrees of freedom also crudely shows that the residual variances of both model (for the East and North components) are not statistically different at the 95% confidence level. In this regard, both models fit the horizontal plate motion captured by the data equally as well as one another.

In both cases, the mean of the residuals in the up direction **is** statistically different from 0 at the 95% confidence level. The residuals of the fitted spherical rotation matrix have a mean of -0.65 mm/yr with a standard deviation of 0.44 mm/yr for the "up" component and the residuals of the fitted ellipsoidal model (again of the "Geodetic Coordinate Ellipsoidal Rotation Matrix Eq. 2.3 i" type) have a mean of -0.81 mm/yr with a standard deviation of 0.45 mm/yr. However, a paired sample t-test indicates that the difference in the means -0.81 and -0.65 mm/yr is significant at the

95% confidence level (with T-statistic $\frac{|-0.81-(-0.65)|}{\sqrt{\frac{0.44^2+0.45^2}{2}}\sqrt{\frac{2}{64}}} = 2.03$). The improvement offered by the ellipsoidal rotation matrix is significant in this context.

Tables 7 and 8 demonstrate that (i) the conventional Euler pole model introduces a systematic height change of 0.16 mm/yr over the Indo-Australian plate and that (ii) this effect is removed when using ellipsoidal rotation matrices (of the "Geodetic Coordinate Ellipsoidal Rotation Matrix Eq. 2.3 i" type). The geodetic vertical land motion is entirely preserved under the fitted ellipsoidal rotation matrix (Eq. 2.3 g/i). This is achieved by manipulating the geometry of the rotation matrix, following Özdemir (2016), and by including a close analogue of the geodetic height as an additional rotation matrix parameter. The effect is evidenced by the mean of the "up" component of the residuals in Table 6 being identical to the mean vertical velocity of the same data in Table 4 and that of Table 8 being zero. However, the mean of the residuals for the "up" direction is -0.65 mm/y for the fitted spherical plate motion model. In this case, the vertical land motion signal is partially absorbed by the parameters of the fitted conventional Euler pole spherical rotation matrices. If this Euler pole plate motion model were to be used to align coordinates before vertical land motion signals are considered, it would effectively result in a 0.15 mm/yr under representation of the continental scale vertical land motion in the geodetic "up" direction. This agrees with the result demonstrated in Fig 3.1 (b).

The ellipsoidal rotation matrix is more complex to implement than the conventional Euler pole model. This is because the parameter μ of the point being rotated is embedded in the matrix itself. For this reason, the rotation matrix is different for each ellipsoidal "height plane" (i.e. points of constant ellipsoidal height) due to this additional parameterisation. However, it is computed readily once the parameters $\boldsymbol{v}$ have been estimated. In contrast, the ellipsoidal rotation matrix given by Eq. 2 c. is the same for all "height planes" and is therefore as simple to implement as the conventional Euler pole model. For completeness, results of fitting the more simplistic form of the ellipsoidal rotation matrix given by Eq. 2 c. have also been included in Tables 6 & 8. Similar to the result of fitting Eq. 2.3. i, the Tables show that it too overcomes some of the issues introduced by the Euler pole model, with respect to the model introducing ellipsoidal height velocities. Generally speaking the results demonstrate that, in the Indo-Australian plate setting it offers half the benefit of the full ellipsoidal rotation matrix (i.e. that of the form of Eq. 2.3 i), introducing a bias of only ~0.08 mm/yr (on average across the GNSS sites) in the ellipsoidal height velocities.

5. Conclusion

When conducting high-precision (mm/yr) vertical land motion studies, it is important to exercise caution when aligning dynamic coordinates from different time periods using a conventional Euler pole plate motion model. The GDA2020 and ATRF datums are underpinned by a plate motion model of this type and it can introduce inaccuracies in geodetic upward velocities of up to -0.2 mm/yr.

The conventional Euler pole plate motion model is effectively a spherical rotation matrix. An alternative rotation matrix, which rotates coordinates along paths

tangent to the ellipsoid has been presented. Both the spherical and ellipsoidal rotation matrices have been fitted to all 841 data points in the ITRF2014 solution on the Indo-Australian tectonic plate and separately to 65 high-quality velocity estimates, to parameterise the tectonic plate motion present in the data.

The full ellipsoidal model (Eq. 2.3. i) is more complex and requires additional considerations to implement (e.g. the addition of the μ coordinate in the rotation matrix) while the simplistic form (Eq. 2.3. c) is as simple as the conventional Euler pole model. Statistically, fitted spherical and both ellipsoidal models perform equally as well in the horizontal directions in the Indo-Australian setting. However, the simplistic ellipsoidal model better preserves the known, continent scale, vertical velocity of the Indo-Australian tectonic plate while the full ellipsoidal model preserves it precisely. For this reason, if a static datum must be used, the full ellipsoidal plate motion model is arguably the preferable choice to align time dependent coordinates horizontally – for broad scale, small amplitude vertical land motion studies.

Open Research

The data files used in this paper are available at Altamimi et al. (2017), Bird (2003) and Geoscience Australia (2021).

References

Altamimi, Z., Rebischung, P., Métivier, L., & Collilieux, X., 2016. ITRF2014: A new release of the International Terrestrial Reference Frame modelling nonlinear station motions. Journal of Geophysical Research: Solid Earth, 121(8), 6109-6131. [Dataset] doi:10.1002/2016JB013098.

Altamimi, Z., Métivier, L., Rebischung, P., Rouby, H., Collilieux, X., ITRF2014 plate motion model, Geophysical Journal International, Volume 209, Issue 3, June 2017, Pages 1906–1912, https://doi.org/10.1093/gji/ggx136

Bird, P., 2003, An updated digital model of plate boundaries Geochemistry Geophysics Geosystems, 4(3), 1027, [Dataset] doi:10.1029/2001GC000252

Blewitt, G., Treatise on Geophysics, 2nd edition, 2015, vol. 3, pp. 307-338, https://doi.org/10.1016/B978-044452748-6.00058-4.

Cheng, M.K., Tapley, B.D., Ries, J.C., 2010, Geocenter Variations from Analysis of SLR data, IAG Commission 1 Symposium 2010, Reference Frames for Applications in Geosciences (REFAG2010), Marne-La-Vallee, France, 4-8 October 2010.

Claessens, S., 2006. Solutions to ellipsoidal boundary value problems for gravity field modelling (Doctoral dissertation, Curtin University).

Cox. A., and Hart, R.B., 1986, Plate tectonics: How it works, Blackwell, p.63-84.

Cuffaro, M., Caputo, M., and Doglioni, C., 2008, Plate subrotations, Tectonics, 27, TC4007, doi:10.1029/2007TC002182.

Featherstone WE, McCubbine JC, Brown NJ, Claessens SJ, Filmer MS, Kirby JF, 2018, The first Australian gravimetric quasigeoid model with location-specific uncertainty estimates. Journal of Geodesy 92(2): 149-168. https://doi.org/10.1007/s00190-017-1053-7.

Geoscience Australia (accessed 2021), GNSS data from Geoscience Australia's National Positioning Infrastructure. Retrieved from https://data.gnss.ga.gov.au/

Gross, R., Beutler, G., and Plag., H.-P., 2009, Integrated scientific and societal user requirements and functional specifications for the GGOS, in Global Geodetic Observing System: Meeting the Requirements of a Global Society on a Changing Planet in 2020, edited by H.-P. Plag and M. Pearlman, pp. 209–224, Springer Berlin, doi:10.1007/978-3-642-02687-4_7.

Heiskanen, W.A. and Moritz, H., 1967. Physical geodesy (Book on physical geodesy covering potential theory, gravity fields, gravimetric and astrogeodetic methods, statistical analysis, etc).

ICSM, 2020, ATRF Technical Implementation Plan, Version 2.3. https://www.icsm.gov.au/sites/default/files/2020-02/ATRF%20Technical%20Implementation%20Plan%20v2.3_1.pdf (last accessed 02/2023)

ICSM, 2021, Geocentric Datum of Australia 2020 Technical Manual, Version 1.6. https://www.icsm.gov.au/sites/default/files/2021-04/GDA2020%20Technical%20Manual%20V1.6.pdf (last accessed 08/2021)

Moritz, H. 2000, Geodetic Reference System 1980, Journal of Geodesy, 74(1)

Nield, G. A., King, M. A., Steffen, R., Blank, B. 2022. A global, spherical finite-element model for post-seismic deformation using Abaqus, Geosci. Model Dev., 15(6), 10.5194/gmd-15-2489-2022

Özdemir, M., 2016. An alternative approach to elliptical motion. Advances in Applied Clifford Algebras, 26(1), pp.279-304.

Pollitz, F. 1997. Gravitational viscoelastic postseismic relaxation on a layered spherical Earth, Journal of Geophysical Research: Solid Earth, 102 (B8), 10.1029/97JB01277

Rezvani, MH., Watson, C.S. & King, M.A. 2022, Vertical deformation and residual altimeter systematic errors around continental Australia inferred from a Kalman-based approach. J Geod 96, 96. https://doi.org/10.1007/s00190-022-01680-3

Riddell, A. R., King, M. A., & Watson, C. S., 2020. Present-day vertical land motion of Australia from GPS observations and geophysical models. Journal of Geophysical Research: Solid Earth, 125(2), e2019JB018034.

Sun, Y., Riva, R., and Ditmar, P., 2016, Optimizing estimates of annual variations and trends in geocenter motion and J2 from a combination of GRACE data and geophysical models, J. Geophys. Res. Solid Earth, 121, doi:10.1002/2016JB013073.

Swenson, S.; Chambers, D. & Wahr (2008), J. Estimating geocenter variations from a combination of GRACE and ocean model output J. Geophys. Res., 113, 8410